

Artificial antiferromagnetic tunnel junction sensors based on Co/Ru/Co sandwiches

C. Tiusan, M. Hehn, K. Ounadjela, Y. Henry, J. Hommet, and C. Meny
Institut de Physique et Chimie des Matériaux de Strasbourg, 23 rue du Loess, F-67037 Strasbourg, France

H. van den Berg, L. Baer, and R. Kinder
Siemens AG, ZT MFI, Paul Gossenstrasse 100, Erlangen D-91052, Germany

A novel method is used for pinning the magnetization of the magnetically hard subsystem in micron-size magnetic tunnel junctions: the so-called artificial antiferromagnetic structure. The latter uses the strong antiparallel exchange coupling between two Co layers through a Ru spacer layer to ensure a high rigidity of the hard subsystem magnetization. The tunnel barriers were formed by sputter etching previously deposited Al layers in a rf Ar/O₂ plasma. Wafers, 3 in. in diameter, were patterned into arrays of square junctions with lateral sizes of 20 and 50 μm . All junctions of a given size show resistances reproducible within several percents. The tunnel magnetoresistance (TMR) is found to be independent of the junction size and TMR ratios of 14%–16% are achieved at room temperature. © 1999 American Institute of Physics. [S0021-8979(99)49508-8]

Following the finding of large magnetoresistance effects at room temperature in three-layer magnetic tunnel junctions (MTJs),¹ spin polarized tunneling, discovered more than 2 decades ago, has recently regained much attention. The tunneling probability of electrons, hence the resistance of magnetic tunnel junctions, is controlled by the relative orientation of the magnetization of the ferromagnetic electrodes having, respectively, a minimum and a maximum value for the parallel and antiparallel alignment of the magnetic moments of the two ferromagnetic layers. The field window between these two extreme states is determined by the difference in the reversal fields of the two magnetic electrodes. It defines the range of field in which a magnetic sensor using a MTJ as an active part may operate efficiently.

In this article, we report on the tunnel magnetoresistance (TMR) of spin dependent tunneling structures using a so-called artificial antiferromagnetic structure (AAF) as a magnetically hard subsystem. These appear as possible alternatives to the commonly used exchange-biased systems, in which the magnetic rigidity of the ferromagnetic reference hard layer is achieved by coupling it to an antiferromagnetic medium.² Its counterpart—the AAF—contains two Co films that are strongly antiferromagnetic through a nonmagnetic Ru interlayer, thus providing a subsystem with very low magnetic moment in the operating field regime. This moment reduction gives an enhancement in the AAF stiffness as compared to the single Co layer of the AAF. Thus angle sensors have been realized with TMR ratios of 14%–16% and field windows larger than 250 Oe at room temperature.

The entire growth of the tunnel junctions was done *in situ*, in a high vacuum sputtering system, having a base pressure of 5×10^{-8} mbar. The multilayers were deposited on Si(111) wafers, beginning the deposition with a Cr(15 Å)/Fe(60 Å)/Cu(300 Å) buffer, which allows us to achieve a reasonable AAF surface roughness, and finishing it with a protective Cu(100 Å)/Cr(50 Å) cap. A typical layer sequence in the active part of the junctions is Co(18 Å)/Ru(8 Å)/Co(30 Å)/Al₂O₃/Co(10 Å)/Fe(60 Å). The asymmetric Co/

Ru/Co sandwich (AAF structure) is the hard subsystem, while the Co/Fe bilayer is the magnetically soft detection subsystem.

By using a Cr/Fe/Cu buffer layers, a reasonable AAF surface roughness was achieved (peak to peak and rms values of 8 and 1.8 Å, respectively), irrespective of the Ru and Co layer thickness. Notice that a significant increase of the surface roughness was eventually observed after the formation of the Al oxide layer on top of the AAF subsystem. The peak to peak and rms roughness then reached 13 and 3 Å, respectively.

For oxidizing the barrier we used a plasma oxidation technique which allows the process to be carried out within a standard commercial sputtering plant without the need of breaking the vacuum or accessing a separate chamber. An Al layer is first deposited. The latter then serves as a cathode for generating a rf Ar/O₂ plasma. A competition thus occurs at the Al surface between sputter etching by Ar ions and oxidation by oxygen ions, which leads to a self-limited oxidation process. In this study, the rf power density was set to 0.05 W/cm², the partial pressure of both Ar and O₂ gases to 9×10^{-3} mbar, and the oxidation time to 1 min.

X-ray photoelectron spectroscopy (XPS) experiments were carried out to extract information first on the chemical composition of the barrier, and second on determining the optimum Al thickness required to avoid under and overoxidation of the barrier, which are both known to result in detrimental effects on the magnetotransport properties of tunnel junctions.⁴ XPS spectra were recorded around the Al 2*p*, O 1*s*, and Co 2*p*_{3/2} and 2*p*_{1/2} peaks on test samples consisting of 100 nm thick layers of Al deposited on Si substrates as well as Si/Cr(15 Å)/Fe(60 Å)/Cu(300 Å)/Co(18 Å)/Ru(8 Å)/Co(30 Å)/Al(oxidized or not)/Ru(50 Å) dummies. Strikingly, these experiments on both types of samples revealed that the direct deposition of Al at a rate of 0.1 Å/s contained a large and nonreproducible amount of oxygen. Indeed, a systematic presence of 2*p* Al peaks located at 76 and 73 eV correlated with the O 1*s* peak revealed the presence of a considerable

amount of Al oxide even after fully etching the 100 nm Al thick film in the XPS chamber. We attribute this to the extremely high reactivity of Al in the presence of water. Most of the residual gas pressure in our sputtering plant is indeed due to water vapor (partial pressure of 2×10^{-8} mbar). Nevertheless, Ar/O₂ plasma oxidation was performed to improve the chemical homogeneity of the Al oxide layer. XPS then showed that an optimal Al thickness of 25 Å oxidized for 1 min allows us to avoid the presence of metallic Al pinholes as well as the oxidation of the topmost AAF Co layer.

In the present hard-soft sensor architecture, a so-called AAF structure is incorporated in order to enhance the magnetic rigidity of the hard subsystem. The AAF consists of two Co layers, with different thicknesses, that are antiferromagnetically coupled by Ruderman-Kittel-Kasuya-Yosida (RKKY)-like interactions through an 8 Å Ru spacer layer. The operational field window of the sensor is located at the field plateau at which the moments \mathbf{m}_1 and \mathbf{m}_2 of the two Co layers are opposite. The plateau width H_p is given by $(m_1 - m_2)/(m_1 + m_2) H_s$, where H_s is the saturation field of the AAF. The room temperature magnetization curve of Fig. 1(a) of a complete stack, including the Fe seed layer and the top electrode (detection layer) clearly shows the plateaus as the horizontal segments with width $H_p \approx 1.5$ kOe at the descending field branches. At the plateaus, the magnetizations of both Co layers are mutually firmly coupled by the interlayer-exchange coupling across the Ru interlayer with strength J_{Ru} and each layer is uniformly magnetized. J_{Ru} is estimated to be 0.6 erg/cm² by the relation $MH_s = -J_{Ru}(d_1 + d_2)/(d_1 d_2)$,⁵ where M is the saturation magnetization and d_1 (respectively d_2) is the thickness of the Co layers. Figure 1(a) also shows that upon reversing the field the uniformity of the Co layers become disturbed at a field H_r of 500 Oe, being significantly smaller than H_p , and that the AAF switches to the plateau with opposite polarity of $\mathbf{m}_1 - \mathbf{m}_2$. The width H_o of the operational field window however depends on H_r rather than on H_p , illustrating that H_o is smaller than H_p . The big gain in the rigidity by the AAF becomes evident by comparing H_r with the coercivity of the Co single layer, being typically 100 Oe or smaller [Fig. 1(b)]. The rigidity of the single Co layers stems from the frictional torque's originating in the microscopic (local) anisotropy of the randomly oriented crystallites that the layers are made of and they do not exhibit any pronounced macroscopic magnetic anisotropy in the plane of the films. This stiffness enhancement is roughly given by the ratio Q of the total magnetic moments of the AAF at saturation and the plateau, i.e., by the relation $Q = (m_1 + m_2)/(m_1 - m_2) \approx (d_1 + d_2)/(d_1 - d_2)$ (Ref. 5) being 4 for the stack of Fig. 1(a), in agreement between experimental finding.

The inset of Fig. 1(a) shows low field minor $M-H$ loops in which only the Fe seed layer ($H_C \sim 19$ Oe) and soft detection layer reverse their magnetization. The minor loop measured after demagnetizing the multilayers (including the AAF) is symmetrical. It reveals that the intrinsic coercivity of the detection layer is 12 Oe. In contrast, the rectangular hysteresis loop of the detection layer at a well aligned AAF magnetization (applied field $< H_o$) is shifted by -4 Oe with respect to the adjustment field of the AAF. This shift re-

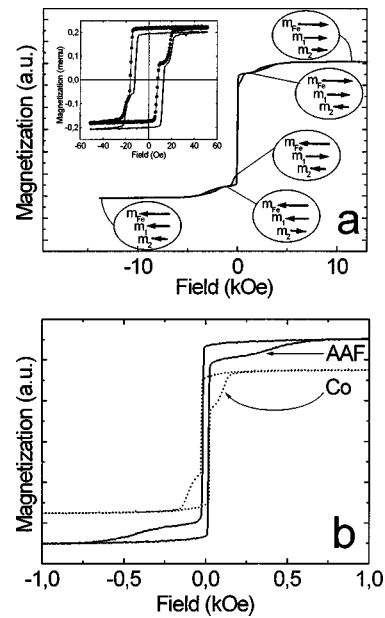


FIG. 1. (a) Room temperature magnetization curve measured on a blanket multilayer film consisting of the MTJ structure. Schematically shown are the successive magnetic configurations along the decreasing field branch. \mathbf{m}_1 , \mathbf{m}_2 , and \mathbf{m}_{Fe} stand for the magnetic moments of the top AAF Co layer, the bottom AAF Co layer, and the detection layer, respectively. (Inset) Minor magnetization loops measured after demagnetizing the multilayer (—) and saturating it along the positive field direction (— · —). The two jumps are attributed to the reversal of the magnetization of the Fe seed layer ($H_C \sim 19$ Oe) and Co/Fe detection bilayer ($H_C \sim 12$ Oe). A ferromagnetic coupling exists between \mathbf{m}_1 and \mathbf{m}_{Fe} which gives rise to a -4 Oe shift of the detection layer loop after saturation of the multilayer magnetization. (b) Room temperature magnetization curves measured on a single 30 Å Co layer (· · ·) and a Co(18 Å)/Ru(8 Å)/Co(30 Å) sandwich (—) grown on Si/Cr(15 Å)/Fe(60 Å)/Cu(300 Å) templates.

verses when the adjustment field is applied in the opposite direction, signifying a coupling between AAF and the detection layer. This coupling has a ferromagnetic nature since the AAF layer closest to the barrier has its \mathbf{m} parallel to the adjustment field and its strength is on the order of 5×10^{-3} erg/cm². This coupling may be attributed to the orange-peel effect⁸ originating in a coherent corrugation of the top and bottom interfaces of the barrier. An estimate of an average amplitude of 7 Å of the top and bottom interface and a lateral characteristic length of typically 300 Å of the corrugation pattern using Néel's model gives indeed a bias field of about 5 Oe, in agreement with the AFM observations.

For transport measurements, as-deposited 3 in. wafers were patterned in four ultraviolet (UV) lithography-etching steps into large arrays of junctions with a square shape tunnel barrier of nominal surface areas $S = 20 \times 20$ and $50 \times 50 \mu\text{m}^2$. Over 50 randomly chosen junctions, dispersed on the wafer, had their magnetoresistance loop and zero field current-voltage ($I-V$) characteristic measured at room temperature using a conventional four point technique with dc bias voltage. All of the measured junctions were free of disease and exhibited nonlinear $I-V$ curves as predicted by tunnel conduction theories. As can be seen in Fig. 2(a), the variation of the current density, $J = I/S$, with the bias voltage is nearly the same for the two junction areas. Thus, the pro-

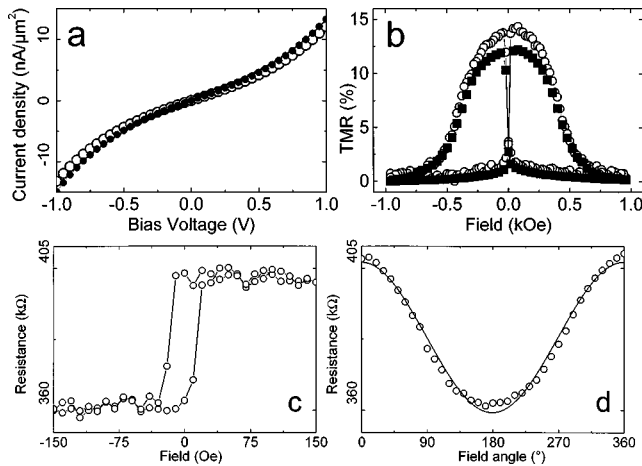


FIG. 2. (a) Current density as a function of bias voltage for tunnel junctions with surface areas of (○) $20 \times 20 \mu\text{m}^2$ and (●) $50 \times 50 \mu\text{m}^2$. (b) Tunnel magnetoresistance loops recorded on a $20 \times 20 \mu\text{m}^2$ junction with bias voltages of (○) 3 mV and (■) 165 mV. (c) Minor resistance loop measured on a $20 \times 20 \mu\text{m}^2$ junction with a 30 mV bias voltage. Changes in tunnel resistance are only due to the reversal of the detection layer. (d) Variation of the tunnel resistance when rotating the applied magnetic field (80 Oe) in the plane of the junction ($V=100$ mV). The experimental data (○) are well fit using a cosine function (—).

portionality of the tunnel conductance to S is verified. Although the investigated devices were not necessarily close to each other on the wafer, the measured resistance proved to be fairly reproducible. Indeed, the resistance data are scattered by only 8% and 4%, respectively, around the average resistance values of 380 k Ω ($20 \times 20 \mu\text{m}^2$) and 60 k Ω ($50 \times 50 \mu\text{m}^2$). These average values lead to a resistance-area product of about 150 M $\Omega \mu\text{m}^2$.

Brinkman's theory of tunneling⁷ was applied to estimate the effective barrier height and thickness. Good fits of the J - V curves to the form given by this theory were obtained. The deduced barrier height of 2.6 eV is in reasonable agreement with results published previously.⁴ As for the estimated barrier thickness of 13.5 Å, it is significantly smaller than the nominal thickness of the deposited Al film (25 Å). A possible explanation for this apparent discrepancy is the following. As mentioned before, corrugations at the top and bottom barrier interfaces might be correlated and the roughness of the top interface is significantly larger than that of the bottom one. Therefore, places might exist where the barrier thickness would be locally reduced as compared to the average Al oxide thickness. Because of the exponential dependence of the tunneling probability with the barrier thickness, such places would have much higher tunnel transmission. Hence, they might transmit most of the tunnel current, leading to a reduced effective barrier thickness.

The room temperature field dependence of the junction resistance was measured for different bias voltages [Fig.

2(b)]. At low bias, typically 3 mV, TMR ratios range from 14% to 16%, with no correlation with the size or the location of the devices on the wafers. Furthermore, it is noteworthy that TMR is found only weakly dependent on the bias voltage. Figure 2(b) presenting magnetoresistance loops of a typical $20 \times 20 \mu\text{m}^2$ junction reveals indeed a slight reduction of the TMR ratio from 15% to 12% as the applied voltage increases from 3 to 165 mV. This result, together with the high voltage value at which the breakdown of most junctions was observed to occur (about 1.8 V), are commonly considered as proofs of good quality tunnel barriers.⁸

In conclusion, the possibility of using magnetic tunnel junctions, containing AAF structures as magnetically hard subsystems, in high-impedance magnetic sensors with large field windows is demonstrated. In fields up to 250 Oe, the AAF subsystem behaves as a truly rigid magnetic body [Fig. 1(b)]. Consequently, changes in the resistance of the junctions in the -250 – 250 Oe field range are solely due to the reversal of the magnetization of the detection layer. This is clearly illustrated in Fig. 2(c), showing that the rectangular shaped magnetoresistance loop associated with this reversal is surrounded by two plateaus. The variation of the TMR in a rotating field, whose strength (80 Oe) was chosen within the operational field window, is shown in Fig. 2(d). The reference direction for the field angle θ was selected antiparallel to the net magnetic moment of the AAF structure. An overall change in resistance of 13% is achieved with a bias voltage of 100 mV. Moreover the TMR follows quite well the $\cos(\theta)$ variation expected for a perfectly frozen AAF subsystem and a freely rotating detection electrode. Using two of these tunnel junctions with orthogonal AAF magnetization should allow us to build 360° angle detectors⁷ having high impedance.

This work was partially supported by the European Community Brite Euram project "Hot Spin Electronics Amplifiers for Magnetic Sensors" (Grant No. BE96-3407). The authors thank Victor Da Costa for helpful discussions.

¹J. S. Moodera, L. R. Kinder, T. M. Wong, and R. Meservey, *Phys. Rev. Lett.* **74**, 3273 (1995); T. Miyazaki and N. Tezuka, *J. Magn. Magn. Mater.* **139**, L231 (1995).

²See e.g., W. J. Gallagher *et al.*, *J. Appl. Phys.* **81**, 3741 (1997).

³A spurious geometrical enhancement of the TMR effect is likely to occur if the resistance of the barrier is too small as compared to that of the current leads. See e.g., R. M. J. van de Verdoonk, J. Nowak, R. Meservey, J. S. Moodera, and W. J. M. de Jonge, *Appl. Phys. Lett.* **71**, 2839 (1997).

⁴J. S. Moodera, E. F. Gallagher, K. Robinson, and J. Nowak, *Appl. Phys. Lett.* **70**, 3050 (1997).

⁵H. A. M. van den Berg, W. Clemens, G. Gieres, G. Rupp, M. Vieth, J. Wecker, and S. Zoll, *J. Magn. Magn. Mater.* **165**, 524 (1997).

⁶L. Néel, *C. R. Acad. Sci. URSS* **255**, 1676 (1962).

⁷W. F. Brinkman, R. C. Dynes, and J. M. Rowell, *J. Appl. Phys.* **41**, 1915 (1971).

⁸J. S. Moodera, J. Nowak, and R. J. M. van de Veerdonk, *Phys. Rev. Lett.* **80**, 2941 (1998).